BIOPHYSICS

The conduction pathway of potassium channels is water free under physiological conditions

Carl Öster[1]*, Kitty Hendriks[1]*, Wojciech Kopec[2], Veniamin Chevelkov[1], Chaowei Shi[1], Dagmar Michl[1], Sascha Lange[1], Han Sun[3], Bert L. de Groot[2], Adam Lange[1,4†]

Ion conduction through potassium channels is a fundamental process of life. On the basis of crystallographic data, it was originally proposed that potassium ions and water molecules are transported through the selectivity filter in an alternating arrangement, suggesting a "water-mediated" knock-on mechanism. Later on, this view was challenged by results from molecular dynamics simulations that revealed a "direct" knock-on mechanism where ions are in direct contact. Using solid-state nuclear magnetic resonance techniques tailored to characterize the interaction between water molecules and the ion channel, we show here that the selectivity filter of a potassium channel is free of water under physiological conditions. Our results are fully consistent with the direct knock-on mechanism of ion conduction but contradict the previously proposed water-mediated knock-on mechanism.

INTRODUCTION

Potassium (K^+)–selective channels allow for the selective and efficient conduction of K^+ ions across the cell membrane. They are involved in numerous physiological and pathophysiological processes (*1*). K^+ channels have been characterized in great detail by numerous studies using electrophysiology, x-ray crystallography, molecular dynamics (MD) simulations, and spectroscopic approaches. The first atomic resolution structure of a K^+ channel was determined around 20 years ago for the channel KcsA, explaining many phenomena observed experimentally before (*2*, *3*). KcsA has become a textbook example of how a protein structure can explain protein function. A selectivity filter (SF), comprising four K^+ binding sites, is formed in the homotetrameric arrangement by segments of the four subunits with the signature sequence TVGYG (Fig. 1A). This narrow pore allows for high selectivity and near diffusion–limited conduction rates. Despite these achievements, some elementary properties of the K^+ channel remain under debate. For example, it was proposed early on that water molecules are cotransported with K^+ ions and that the conduction through the SF occurs via alternating water molecules and ions in a mechanism that we refer to in the following as "water-mediated" knock-on (*4*). This mechanism involves a cycle of [W, K, W, K], where W refers to water and K, is K^+, and [K, W, K, W] states occupying the SF binding sites S1 to S4 (Fig. 1, A and B).

The water-mediated knock-on mechanism had been the accepted model in the field until 2014 when a study suggesting that ions are in direct contact with each other and that no water molecules are involved in the conduction process appeared (*5*). The proposed "direct" knock-on mechanism (Fig. 1C) (*5*) was first observed in computational electrophysiology simulations of KcsA and furthermore supported by reanalysis of x-ray crystallographic data, indicating that, also under crystallographic conditions, adjacent binding sites are simultaneously occupied by K^+ ions. More recently, the latter result was confirmed by anomalous x-ray diffraction studies of the K^+ channel NaK2K (*6*). NaK2K is a K^+-selective double mutant (D66Y and N68D) of the nonselective channel NaK and a well-established model system for K^+-selective channels (*7*, *8*). In contrast, a recent investigation using two-dimensional (2D) infrared (IR) spectroscopy appeared to favor the water-mediated rather than the direct knock-on mechanism (*9*).

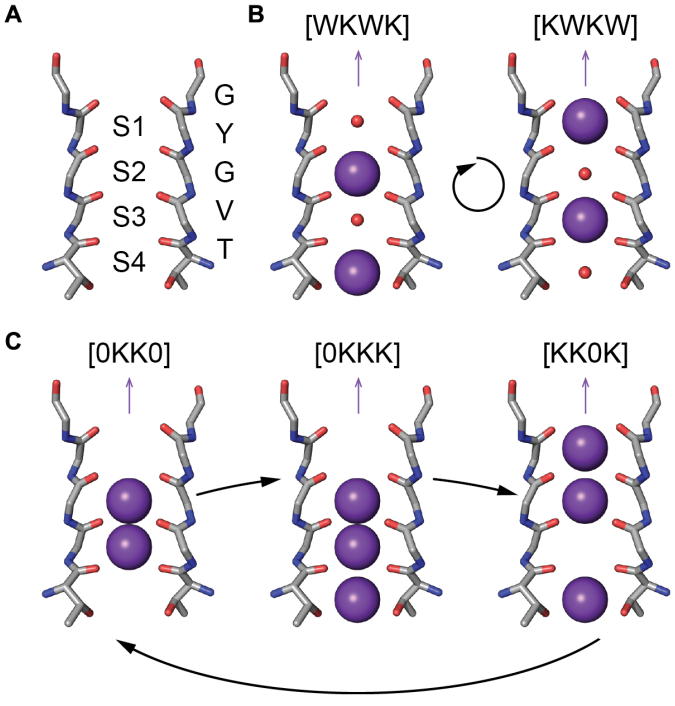

Fig. 1. Comparison between water-mediated and direct knock-on ion permeation mechanisms. (**A**) The structure of the SF in NaK2K [Protein Data Bank (PDB) ID: 3ouf], with the ion binding sites (S1 to S4) and amino acid sequence indicated. (**B**) The two stages of the water-mediated knock-on mechanism. (**C**) The three stages of the direct knock-on mechanism. K^+ ions and water molecules are displayed as purple and small red spheres, respectively. The name of the state is indicated above the structure, showing the occupancy at binding sites S1 to S4 with either K^+ (K) or water (W), or unoccupied (0).

[1]Department of Molecular Biophysics, Leibniz-Forschungsinstitut für Molekulare Pharmakologie, 13125 Berlin, Germany. [2]Biomolecular Dynamics Group, Max Planck Institute for Biophysical Chemistry, 37077 Göttingen, Germany. [3]Section Structural Biology, Leibniz-Forschungsinstitut für Molekulare Pharmakologie, 13125 Berlin, Germany. [4]Institut für Biologie, Humboldt-Universität zu Berlin, 10115 Berlin, Germany.
*These authors contributed equally to this work.
†Corresponding author. Email: alange@fmp-berlin.de

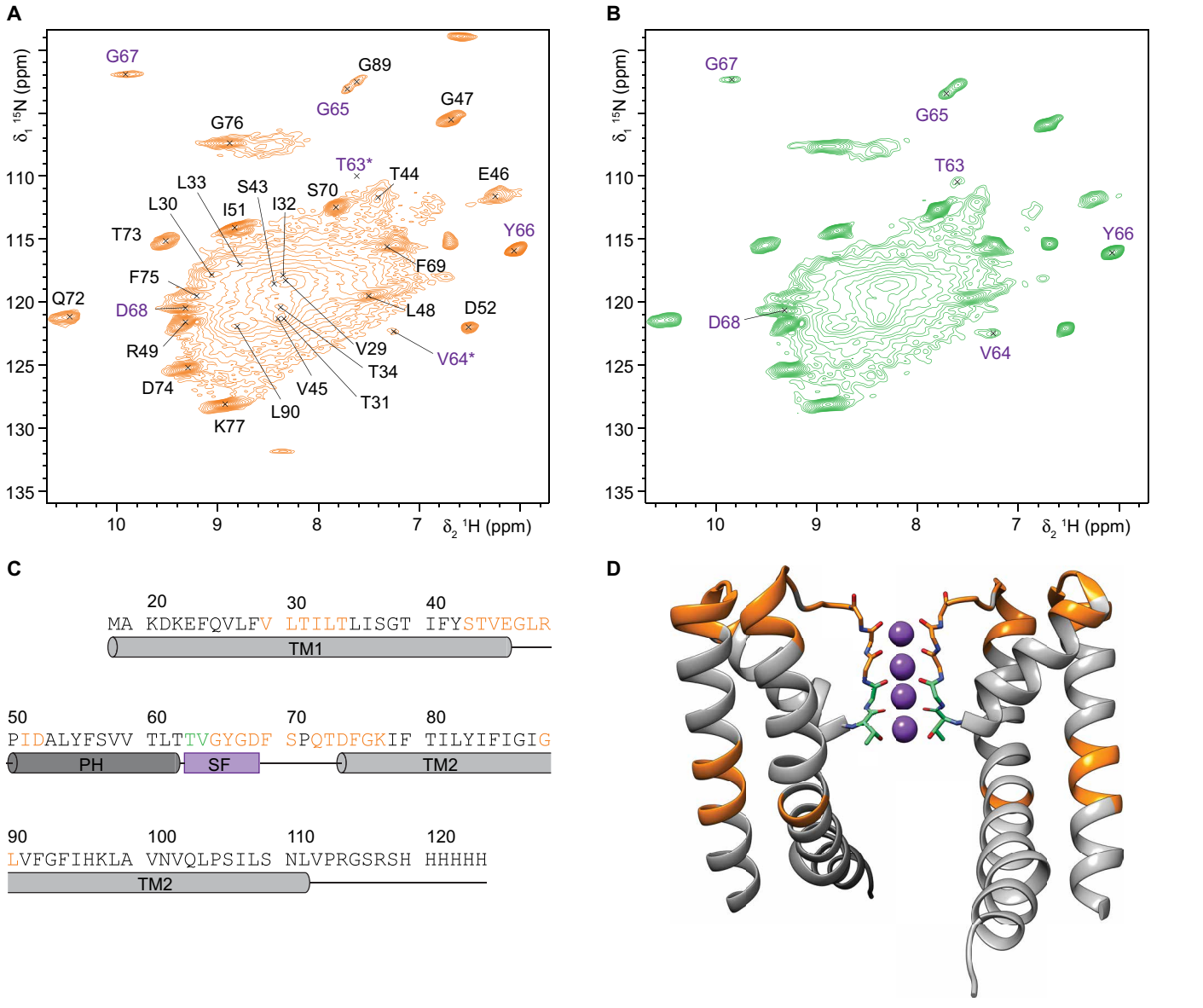

Fig. 2. Assignment of back-exchanged deuterated NaK2K. (**A**) CP-based NH spectrum of NaK2K, with the peak assignment indicated and with SF residues in purple. (*) T63 and V64 are indicated but could only be assigned on the basis of the spectra recorded after the washing procedure. ppm, parts per million. (**B**) CP-based NH spectrum of NaK2K, after the washing procedure, with assignments of SF residues indicated. (**C**) Assigned residues are indicated on the protein sequence in orange (based on back-exchanged deuterated NaK2K) and green (based on back-exchanged deuterated NaK2K after the washing procedure). The structural elements are shown underneath the sequence: the TM1, the pore helix (PH), the SF, and the TM2. (**D**) The assigned residues are indicated on the crystal structure of NaK2K (PDB ID: 3ouf) in orange and green (based on back-exchanged deuterated NaK2K before and after the washing procedure, respectively). The binding sites (S1 to S4) are indicated as purple spheres, and for clarity, only two opposing subunits are shown.

However, more recently, it could be shown that the 2D IR data are also in accordance with the direct knock-on mechanism (*10*). Notably, all of these previous investigations were either based on x-ray analysis of detergent-solubilized proteins or MD simulations using the so-obtained structures.

At this stage, it would thus be highly interesting to directly investigate the role of water molecules in the SF experimentally under conditions which are close to the native state. This means, in the context of membrane proteins, to study them embedded in a lipid bilayer at room temperature and under physiological buffer conditions. Solid-state nuclear magnetic resonance (NMR) is a structural biology technique that has emerged over the past two decades and that is quite suitable for this task. Solid-state NMR has already been used successfully to investigate the structure and dynamics of several membrane proteins (*11*, *12*), including the ion channels KcsA-Kv1.3 (*13*), wild-type KcsA (*14*, *15*), VDAC (voltage-dependent anion channel) (*16*), M2 (*17*, *18*), and NaK and NaK2K (*19*). Furthermore, it has been demonstrated that solid-state NMR can probe the interaction of the protein of interest

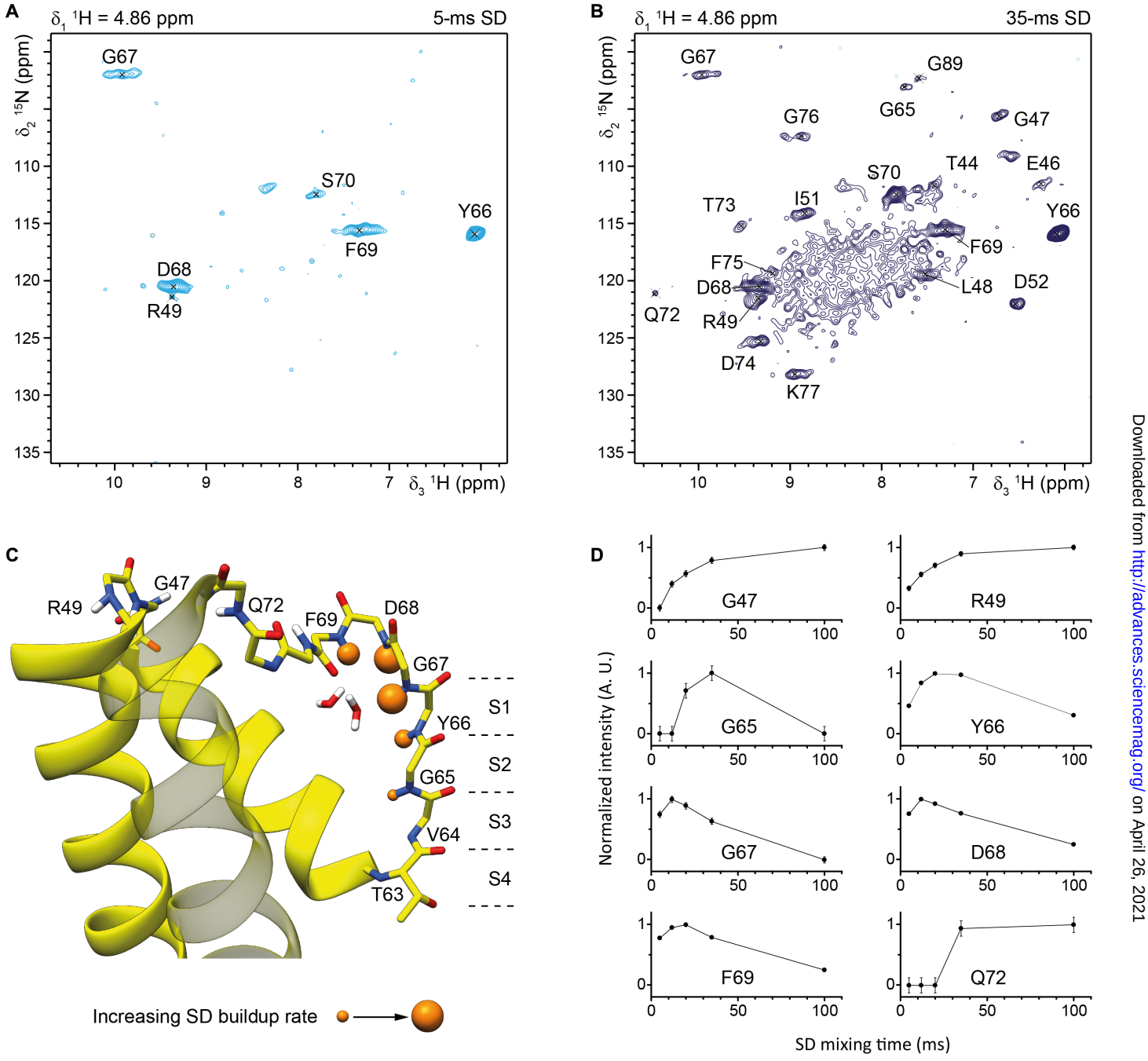

Fig. 3. Spin diffusion buildup from bound water to amide protons in NaK2K. 2D HN slices with mixing times of 5 ms (**A**) and 35 ms (**B**) taken at the chemical shift of bound water (4.86 ppm) from 3D H(H)HN spin diffusion experiments. (**C**) Close up around the SF in a monomer of the tetrameric NaK2K structure (PDB ID: 3ouf). The magnetization transfer from bound water molecules to amide protons in the SF is indicated as orange spheres, where larger spheres represent faster spin diffusion buildup rates. S1 to S4 represent the binding sites in the SF. (**D**) Spin diffusion buildup plots from bound water to amide protons for the indicated residues. The error bars are based on the average noise levels in the 3D spectra. A.U., arbitrary unit; SD, spin diffusion.

with water molecules, for instance by hydrogen/deuterium (H/D) exchange experiments, which are sensitive to processes occurring on long time scales, i.e., seconds to hours or even days (*20*). In addition, ^{1}H spin diffusion experiments allow for the detection of bound water molecules, which interact with the protein on a shorter time scale of 1 to 100 ms, via magnetization exchange (*21*, *22*). Here, we have investigated the K^{+} channel NaK2K (*23*) by ^{1}H-detected solid-state NMR (*24*–*26*) and MD simulations to investigate whether water molecules are present in its SF under equilibrium conditions, i.e., without an applied voltage.

RESULTS

For this purpose, we prepared a deuterated detergent–solubilized sample with a [^{2}H, ^{13}C, ^{15}N]-labeling scheme and subsequently exposed it to water. Deuterons of water-exposed residues can then exchange to protons in a process known as H/D exchange, making those sites NMR visible. H/D exchange is usually restricted to amide protons (H^N) and some side-chain protons. Figure 2A shows the fingerprint cross-polarization (CP)–based NH correlation spectrum of NaK2K after reconstitution into *Escherichia coli* lipids in the presence of 50 mM K^+ at 25°C. Under these conditions, the spectrum exhibits around 20 to 25 sharp signals, similar to what has been observed before for KcsA (*27*), with a broader feature in the background. The sharp signals could be readily assigned with the help of a set of 3D experiments: (H)COCA(N)H, (H)CACO(N)H, (H)CANH, and (H)CONH (fig. S1 and table S1). We found that the assignable signals correspond to three regions of the protein (Fig. 2, C and D). The strongest and sharpest signals are from the extracellular part (G47-D52 and D68-K77). Furthermore, signals are observed for the upper part of the SF (G65-G67). Weaker signals are also observed for residues around the gating hinge region in transmembrane helix 2 (TM2) (G89 and L90) and for the corresponding residues in TM1 (around L30). As expected, we do not observe any exchange in the protected parts of TM1 and TM2. In addition, most of the SF residues are weak (G65) or missing altogether in the assignment spectra (T63 and V64; backbone ^{13}C and ^{15}N chemical shifts are known from ^{13}C-detected experiments; fig. S2 and table S2), indicating that those regions are not exposed to water. The H/D exchange pattern for the SF is in agreement with previous observations for KcsA, where only Y78 and G79 (corresponding to Y66 and G67 in NaK2K) are water accessible (*27*, *28*), as well as with H/D exchange patterns deduced from MD simulations (fig. S3). This is the first indication that there is no water present in the SF, possibly with the exception of binding site S1, and that binding sites S2 to S4 are instead solely occupied by K^+ at the given concentration in our experimental setting. This observation is corroborated by extended MD simulations performed at 0 mV (fig. S4), in which binding sites S2 and S3 are never occupied by a water molecule, while water in binding site S4 is present less than 20% of the time. To further investigate how the water accessibility depends on ion occupancy in the SF, we washed the sample in a buffer without K^+ ions and subsequently returned the sample to the original condition with 50 mM K^+. In the spectra recorded after the washing steps, residues T63 and V64 show clear peaks (Fig. 2B) and could be assigned on the basis of 3D (H)CANH and (H)CONH experiments. T63 and V64 could now be identified as weak noisy peaks in the 2D NH spectrum of the original sample (Fig. 2A), suggesting that they are very slightly exchanged initially and become strongly water exposed during the washing procedure (fig. S5). Note that the washing procedure does not result in a collapsed state of the SF in NaK2K. K^+ ions are not required to stabilize the SF in the conductive conformation for NaK2K (and other K^+ channels, e.g., MthK) (*7*). This is in contrast to KcsA (and several other K^+ channels) where the SF functions as an inactivation gate (*29*).

In principle, it is unexpected that the region below the gating hinge at G89 in TM2 is not visible because it should be water accessible (see movie S1). However, it may be conceivable that slow dynamics of this part would be present at room temperature in liposomes. These dynamics could indeed lead to line broadening effects. We therefore tentatively assign the broad feature in the spectrum to the protein segments below the hinge region. Corroboration of this assumption comes from an INEPT (insensitive nuclei enhanced by polarization transfer)–based NH correlation experiment where the broad background signal is missing (fig. S6). This result indicates that the region below the hinge is dynamic on a time scale that interferes with the INEPT-based transfer and at the same time leads to line broadening in the CP-based spectrum, suggesting dynamics on the millisecond time scale. If the line broadening had instead been the result of static disorder, then the broad signals would have shown up in the INEPT-based spectrum as well.

Next, we performed an experiment in which magnetization from water is transferred to the protein. The efficiency of the magnetization transfer depends on the distance between bound water and amide protons. When the transfer time is short (5 ms; Fig. 3A), we observe only a few amides, with strong peaks only for residues in and around the SF, and in a spectrum with longer transfer time (35 ms; Fig. 3B), we observe transfer from water to almost all observable amide protons. Depending on the signal buildup behavior (based on five experiments with transfer times of 5, 12, 20, 35, and 100 ms; fig. S7), the residues can be divided into two classes as can be seen in Fig. 3D. The curves of one class, represented by G47, R49, and Q72, build up slowly and do not relax on the investigated time scale. Those amide protons are in close proximity to transiently bound water molecules that are themselves in exchange with the bulk water, which dominates the relaxation behavior. In contrast, the amide protons of residues G65 to F69 build up relatively fast and then decay with a relaxation time that corresponds to rigid protons in the protein (see figs. S8 and S9 for all spin diffusion buildup plots before and after the washing procedure, respectively). Those residues are all in contact with two structural water molecules at the back of the SF as observed in the crystal structure [Protein Data Bank (PDB) ID: 3ouf]. Their buildup rates, visualized in Fig. 3C by spheres of variable size, follow the expected pattern based on the distance of their amide protons to those structural water molecules (table S3), i.e., G67 and D68 build up the fastest, followed by F69, Y66, and lastly G65. This order can only be explained if all the water magnetization comes from the two structural water molecules at the back of the upper SF and not by additional water molecules in the SF. If water molecules were present in the SF as well, as predicted by the water-mediated knock-on mechanism, then a different buildup behavior would be expected. For example, in this case, G65 and Y66 should have shown a buildup comparable to G67 and D68, which are in close proximity to the structural water molecules. Although T63 and V64 are barely visible in the 2D NH spectra, we do observe clear diagonal peaks for those residues in the spin diffusion experiments. No magnetization transfer from water is observed for either T63 or V64, which is consistent with the magnetization transfer from water to the SF residues only coming from the bound water behind the SF. Our results agree well with previous observations for KcsA, where G79 and L81 (corresponding to G67 and F69 in NaK2K) are in close proximity to a bound water molecule (*27*, *30*).

DISCUSSION

In summary, both the H/D exchange results and the water-to-protein magnetization transfer experiments show that there is no water in the central SF binding sites as long as K^+ ions are present at a physiological concentration, preventing water from entering the SF. We note that H/D exchange in the lower part of the SF (T63 and V64) would probably require both the presence of water in the SF and

carbonyl flipping (*29*, *31*) of the SF residues, as this would expose the SF amides to the pore. Another potential explanation could be that the H/D exchange of T63 and V64 comes from the water behind the SF because of structural rearrangements. However, such structural rearrangements would have been detected in crystal structures of NaK2K in the presence and absence of K^+ ions (*7*, *8*). Further, a recent solid-state NMR study on KcsA showed that mutations removing hydrogen bonds and increasing the water accessibility behind the SF did not result in H/D exchange in the lower part of the SF (*32*). In the same study, increased dynamics was shown to be related to carbonyl flipping in the SF. It would thus be interesting to investigate the proximity of water molecules to the SF residues in these mutants. Our data are consistent with increased dynamics during the washing procedure, which would allow water to enter the SF when no ions are present, resulting in H/D exchange in the lower part of the SF. Previous and current results from MD simulations show that both aspects, carbonyl flipping and water in the SF, are linked: If water is present in binding sites S1 to S4, then the corresponding SF residues are prone to frequent flips (figs. S10 and S11) (*33*). Therefore, we can interpret our results such that the K^+ ions prevent H/D exchange in two ways: They stabilize the SF in a conductive, nonflipped conformation and at the same time prevent water binding at the K^+ binding sites. As the upper part of the SF exhibits some degree of H/D exchange, it is likely that binding site S1 is partially occupied by water. In conclusion, our data strongly support the direct knock-on mechanism of ion conduction.

MATERIALS AND METHODS

Sample preparation

The NaK2K construct (NaK D66Y and N68D double mutant; plasmid provided by Y. Jiang) is missing the first 19 amino acids and has a C-terminal hexahistidine tag. The NaK2K construct was cloned from the original pQE60 vector into a pET28a expression vector using the NCO I and Hind III cleavage sites on both plasmids (protein sequence: MAKDKEFQVLFVLTILTLISGTIFYSTVEGLRPIDALYFSV-VTLTTVGDGNFSPQTDFGKIFTILYIFIGIGLVFGFIHKLAVN-VQLPSILSNLVPRGSRSHHHHHH).

The protein was expressed in *E. coli* OverExpress C43(DE3) (Lucigen) using 2 liters of deuterated M9 medium. The cells were adapted to D_2O conditions as described previously (*24*). Deuterated M9 medium (D_2O 99.9% D; D214, Eurisotop) was supplemented with α-ketobutyric acid (60 mg/liter; CDLM-7318-PK, Cambridge Isotope Laboratories), D-glucose ^{13}C (4 g/liter; 552151, Sigma-Aldrich), and lyophilized deuterated ^{15}N ammonium chloride (1 g/liter; 299251, Sigma-Aldrich). At an OD_{600} (optical density at 600 nm) of 0.8, the cultures were induced with 0.4 mM IPTG (isopropyl β-D-1-thiogalactopyranoside) and grown for 24 hours at 25°C. Additional labeled deuterated glucose (1 g/liter) and deuterated $^{15}NHCl$ (0.25 g/liter) were added to the cultures 6 hours after induction. Cells were harvested and resuspended with 10 ml of lysis buffer [50 mM tris (pH 7.5), 100 mM NaCl, 1 mM MgCl, and protease inhibitor cocktail (11836170001, Sigma-Aldrich)] per gram of cell pellet. The sample was lysed using a microfluidizer (LM10, Microfluidics) with five cycles of a working pressure of 15,000 psi. The membrane fraction was isolated by ultracentrifugation at 150,000 relative centrifugal force (rcf) for 2 hours and solubilized in 80 ml of solubilization buffer [50 mM tris (pH 7.5), 100 mM NaCl, and 40 mM DM (n-Decyl-β-maltoside; GLYCON Biochemicals)] at room temperature for 3 hours. The protein was batch-purified by immobilized metal affinity chromatography using 5 ml of bed volume of TALON Superflow beads (GE Healthcare Life Sciences). Protein concentrations were determined using Bradford reagent supplemented with α-cyclodextrin (5 mg/ml; AppliChem), and 5.4 mg of protein was mixed with *E. coli* total lipid extract (100500, Avanti Polar Lipids) in a ratio of 2:1 (w/w). H/D back exchange and proteoliposome formation were performed by dialysis for 8 days at 100× dilution against 500 ml of 100% H_2O with 20 mM tris (pH 8.0) and 50 mM KCl, followed by ultracentrifugation at 300,000 rcf for 4 hours at 4°C. Half of the pellet was removed for NMR experiments (sample A, K^+). The second half of the sample was resuspended in 1 ml of 20 mM tris (pH 8.0) and kept rotating at 4°C. The buffer was refreshed twice over the course of 14 days, each time after ultracentrifugation at 150,000 rcf for 30 min at 4°C.

From this, half of the sample was removed for NMR experiments (sample B, no ions). The other half of the sample was resuspended in 1 ml of 20 mM tris (pH 8.0) with 50 mM KCl. The sample was kept rotating at 4°C for 8 days, during which time the buffer was refreshed once and used for NMR experiments (sample C, washed to K^+).

Solid-state NMR

Sample A (K^+) was packed into a 1.9-mm solid-state NMR rotor (Bruker BioSpin), and 1 μl of D_2O was added to enable deuterium locking. To prevent leakage, a spacer was added between the bottom cap and the sample, and the drive cap was glued using a silicon-based glue. The washed samples [sample B (no ions) and sample C (washed to K^+)] were packed into 1.3-mm rotors (Bruker BioSpin), and the drive caps were glued as well to prevent leakage. Experiments on sample A were recorded at 40-kHz magic angle spinning (MAS) using a four-channel (^1H, ^{13}C, ^{15}N, and ^2H) 1.9-mm probe (Bruker BioSpin) on a spectrometer with an external magnetic field strength corresponding to 900 MHz (Bruker BioSpin). Four CP-based 3D experiments [(H)CANH, (H)CONH, (H)CACO(N)H, and (H)COCA(N)H] were recorded for backbone chemical shift assignments of sample A, closely following earlier work by Fricke *et al.* (*24*). The assigned chemical shifts confirm protein folding into a single dominant conformation. Spin diffusion [H(H)NH] experiments with mixing times of 5, 12, 20, 35, and 100 ms were recorded using a 3D version of the standard (H)NH experiment, with the addition of a ^1H acquisition period followed by a spin diffusion sequence on the ^1H channel (90° pulse, spin diffusion mixing time, 90° pulse) before the CP-based transfer to ^{15}N. A recycle delay of 1 s and 90° pulses of 83.3, 50, and 35.7 kHz for ^1H, ^{13}C, and ^{15}N, respectively, were used for all experiments acquired on sample A. Experiments on samples B and C were recorded at 58- to 60-kHz MAS using a three-channel (^1H, ^{13}C, and ^{15}N) 1.3-mm probe (Bruker BioSpin) on a spectrometer with an external magnetic field strength corresponding to 600 MHz (Bruker BioSpin). For sample B, a 3D (H)CANH spectrum was recorded, and for sample C, 3D (H)CANH and (H)CONH spectra were recorded to identify new peaks compared to sample A. Spin diffusion (H(H)NH) experiments with mixing times of 20, 40, and 60 ms were recorded on sample C. A recycle delay of 1 s and 90° pulses of 100, 50, and 35.7 kHz for ^1H, ^{13}C, and ^{15}N, respectively, were used for all experiments acquired on samples B and C. The chemical shifts were referenced to DSS (4,4-dimethyl-4-silapentane-1-sulfonic acid) using an external reference. The sample temperature was kept at 25°C, as measured from the ^1H chemical shift of water. Proton detection with a 30-ms acquisition time was used for all experiments.

Further experimental parameters for the 3D experiments are listed in tables S4 to S7.

Data analysis

All NMR data were processed using TopSpin 4 and analyzed using NMRFAM (National Magnetic Resonance Facility at Madison)–Sparky (*34*) and CcpNmr Analysis (*35*). High-resolution figures based on 3D structures were produced using PyMOL and UCSF (University of California, San Francisco) Chimera (*36*).

MD simulations

For calculations of the solvent accessible surface area (SASA) and backbone NH hydrogen protection, as well as for the time traces showing the correlation between the water presence in binding site S3 and carbonyl flipping of V64, MD trajectories of NaK2K, as reported in a recent publication (*10*), were used. In short, the high-resolution structure of the open-state NaK2K (PDB ID: 3ouf), with the F92A mutation, was inserted in a POPC (1-palmitoyl-2-oleoyl-sn-glycero-3-phosphocholine) membrane, surrounded with explicit water and K^+ and Cl^- ions, and simulated for 6.5 and 10.5 μs with the Amber99sb and CHARMM36m force fields (*37*–*40*) [labeled as AMBER (Assisted Model Building with Energy Refinement) and CHARMM (Chemistry at Harvard Macromolecular Mechanics) in the current manuscript], respectively, under an applied voltage of 300 mV. All the simulation details can be found in the previous publication (*10*). SASA patterns were calculated using the gmx sasa program, with a probe radius of 0.14 nm, and averaged over all trajectories. The backbone NH hydrogen bond protection patterns report the fraction of frames in which a given NH participated in hydrogen bonding with another protein residue and were calculated using the gmx hbond program over all trajectories.

To calculate the average occupancy of each site at a voltage of 0 mV, 50 frames per force field were randomly selected from the applied voltage simulations and further simulated for additional 200 ns per frame without any voltage, resulting in 10 μs of sampling per force field. All remaining simulation parameters and details were identical to those used for simulations with an applied voltage. The occupancy of each site was calculated with a custom Fortran code.

For simulations and analyses, the GROMACS package was used (*41*–*47*), together with GromacsWrapper (*48*). Visualizations and movies were made with visual molecular dynamics (VMD) (*49*).

SUPPLEMENTARY MATERIALS

Supplementary material for this article is available at http://advances.sciencemag.org/cgi/content/full/5/7/eaaw6756/DC1

Fig. S1. Assignments of back-exchanged deuterated NaK2K in the presence of 50 mM K^+.
Fig. S2. 2D ^{15}N-^{13}Cα correlation spectrum of uniformly (^{13}C and ^{15}N)-labeled NaK2K in the presence of 50 mM K^+.
Fig. S3. Predicted H/D exchange pattern based on MD simulations.
Fig. S4. Occupancies of the main ion binding sites of the NaK2K SF in MD simulations performed without an applied voltage.
Fig. S5. Comparison of 2D (H)NH spectra and illustrations of the washing procedure for back-exchanged deuterated NaK2K.
Fig. S6. Comparison of 2D (H)NH spectra of back-exchanged deuterated NaK2K in the presence of K^+ using through-bond or through-space transfer.
Fig. S7. 2D HN slices from 3D H(H)NH spin diffusion experiments with varying mixing times.
Fig. S8. Spin diffusion buildup plots from bound water (blue circles) to amide protons and between neighboring amide protons (red triangles) in back-exchanged deuterated NaK2K in the presence of 50 mM K^+.
Fig. S9. Spin diffusion buildup plots from bound water (blue circles) to amide protons and between neighboring amide protons (red triangles), recorded after the washing procedure for back-exchanged deuterated NaK2K in the presence of 50 mM K^+.
Fig. S10. The relationship between carbonyl flipping and water presence at S3 in MD simulations under an applied voltage performed with the AMBER force field.
Fig. S11. The relationship between carbonyl flipping and water presence at S3 in MD simulations under an applied voltage performed with the CHARMM force field.
Table S1. Chemical shift assignments of deuterated back-exchanged NaK2K, in the presence of 50 mM K^+, based on ^{1}H-detected solid-state NMR experiments.
Table S2. Chemical shift assignments of NaK2K SF residues, in the presence of 50 mM K^+, based on ^{13}C-detected solid-state NMR experiments.
Table S3. Distances (Å) to amide protons of the SF in NaK2K (PDB ID: 3ouf) from the closest water molecule and binding sites (S1 to S4).
Table S4. Experimental parameters for 3D (H)CANH experiments acquired at 25°C on 100% H_2O back-exchanged uniformly (^{2}H, ^{13}C, and ^{15}N)-labeled NaK2K.
Table S5. Experimental parameters for 3D (H)CONH experiments acquired at 25°C on 100% H_2O back-exchanged uniformly (^{2}H, ^{13}C, and ^{15}N)-labeled NaK2K.
Table S6. Experimental parameters for 3D (H)CACO(N)H and (H)COCA(N)H experiments acquired at 25°C on 100% H_2O back-exchanged uniformly (^{2}H, ^{13}C, and ^{15}N)-labeled NaK2K.
Table S7. Experimental parameters for 3D H(H)NH spin diffusion experiments acquired at 25°C on 100% H_2O back-exchanged uniformly (^{2}H, ^{13}C, and ^{15}N)-labeled NaK2K.
Movie S1. Typical K^+ ion permeation process through NaK2K, observed in a 20-ns trajectory segment of MD simulations under an applied voltage.

REFERENCES AND NOTES

1. B. Hille, *Ionic Channels of Excitable Membranes* (Sinauer, ed. 3, 2001).
2. D. A. Doyle, J. Morais Cabral, R. A. Pfuetzner, A. Kuo, J. M. Gulbis, S. L. Cohen, B. T. Chait, R. MacKinnon, The structure of the potassium channel: Molecular basis of K^+ conduction and selectivity. *Science* **280**, 69–77 (1998).
3. Y. Zhou, J. H. Morais-Cabral, A. Kaufman, R. MacKinnon, Chemistry of ion coordination and hydration revealed by a K^+ channel–Fab complex at 2.0 Å resolution. *Nature* **414**, 43–48 (2001).
4. J. H. Morais-Cabral, Y. Zhou, R. MacKinnon, Energetic optimization of ion conduction rate by the K^+ selectivity filter. *Nature* **414**, 37–42 (2001).
5. D. A. Köpfer, C. Song, T. Gruene, G. M. Sheldrick, U. Zachariae, B. L. de Groot, Ion permeation in K^+ channels occurs by direct Coulomb knock-on. *Science* **346**, 352–355 (2014).
6. P. S. Langan, V. G. Vandavasi, K. L. Weiss, P. V. Afonine, K. el Omari, R. Duman, A. Wagner, L. Coates, Anomalous x-ray diffraction studies of ion transport in K^+ channels. *Nat. Commun.* **9**, 4540 (2018).
7. M. G. Derebe, D. B. Sauer, W. Zeng, A. Alam, N. Shi, Y. Jiang, Tuning the ion selectivity of tetrameric cation channels by changing the number of ion binding sites. *Proc. Natl. Acad. Sci. U.S.A.* **108**, 598–602 (2011).
8. D. B. Sauer, W. Zeng, J. Canty, Y. Lam, Y. Jiang, Sodium and potassium competition in potassium-selective and non-selective channels. *Nat. Commun.* **4**, 2721 (2013).
9. H. T. Kratochvil, J. K. Carr, K. Matulef, A. W. Annen, H. Li, M. Maj, J. Ostmeyer, A. L. Serrano, H. Raghuraman, S. D. Moran, J. L. Skinner, E. Perozo, B. Roux, F. I. Valiyaveetil, M. T. Zanni, Instantaneous ion configurations in the K^+ ion channel selectivity filter revealed by 2D IR spectroscopy. *Science* **353**, 1040–1044 (2016).
10. W. Kopec, D. A. Köpfer, O. N. Vickery, A. S. Bondarenko, T. L. C. Jansen, B. L. de Groot, U. Zachariae, Direct knock-on of desolvated ions governs strict ion selectivity in K+ channels. *Nat. Chem.* **10**, 813–820 (2018).
11. S. Wang, V. Ladizhansky, Recent advances in magic angle spinning solid state NMR of membrane proteins. *Prog. Nucl. Magn. Reson. Spectrosc.* **82**, 1–26 (2014).
12. L. Joedicke, J. Mao, G. Kuenze, C. Reinhart, T. Kalavacherla, H. R. A. Jonker, C. Richter, H. Schwalbe, J. Meiler, J. Preu, H. Michel, C. Glaubitz, The molecular basis of subtype selectivity of human kinin G-protein-coupled receptors. *Nat. Chem. Biol.* **14**, 284–290 (2018).
13. A. Lange, K. Giller, S. Hornig, M.-F. Martin-Eauclaire, O. Pongs, S. Becker, M. Baldus, Toxin-induced conformational changes in a potassium channel revealed by solid-state NMR. *Nature* **440**, 959–962 (2006).
14. K. Varga, L. Tian, A. E. McDermott, Solid-state NMR study and assignments of the KcsA potassium ion channel of *S. lividans*. *Biochim. Biophys. Acta.* **1774**, 1604–1613 (2007).
15. M. P. Bhate, B. J. Wylie, L. Tian, A. E. McDermott, Conformational dynamics in the selectivity filter of KcsA in response to potassium ion concentration. *J. Mol. Biol.* **401**, 155–166 (2010).
16. R. Schneider, M. Etzkorn, K. Giller, V. Daebel, J. Eisfeld, M. Zweckstetter, C. Griesinger, S. Becker, A. Lange, The native conformation of the human VDAC1 N terminus. *Angew. Chem. Int. Ed.* **49**, 1882–1885 (2010).
17. F. Hu, W. Luo, M. Hong, Mechanisms of proton conduction and gating in influenza M2 proton channels from solid-state NMR. *Science* **330**, 505–508 (2010).
18. M. Sharma, M. Yi, H. Dong, H. Qin, E. Peterson, D. D. Busath, H.-X. Zhou, T. A. Cross, Insight into the mechanism of the influenza A proton channel from a structure in a lipid bilayer. *Science* **330**, 509–512 (2010).

19. C. Shi, Y. He, K. Hendriks, B. L. de Groot, X. Cai, C. Tian, A. Lange, H. Sun, A single NaK channel conformation is not enough for non-selective ion conduction. *Nat. Commun.* **9**, 717 (2018).
20. L. Shi, I. Kawamura, K.-H. Jung, L. S. Brown, V. Ladizhansky, Conformation of a seven-helical transmembrane photosensor in the lipid environment. *Angew. Chem. Int. Ed.* **50**, 1302–1305 (2011).
21. H. Van Melckebeke, P. Schanda, J. Gath, C. Wasmer, R. Verel, A. Lange, B. H. Meier, A. Böckmann, Probing water accessibility in HET-s(218–289) amyloid fibrils by solid-state NMR. *J. Mol. Biol.* **405**, 765–772 (2011).
22. D. Huster, X. Yao, M. Hong, Membrane protein topology probed by ^{1}H spin diffusion from lipids using solid-state NMR spectroscopy. *J. Am. Chem. Soc.* **124**, 874–883 (2002).
23. A. Alam, Y. Jiang, High-resolution structure of the open NaK channel. *Nat. Struct. Mol. Biol.* **16**, 30–34 (2009).
24. P. Fricke, V. Chevelkov, M. Zinke, K. Giller, S. Becker, A. Lange, Backbone assignment of perdeuterated proteins by solid-state NMR using proton detection and ultrafast magic-angle spinning. *Nat. Protoc.* **12**, 764–782 (2017).
25. T. Schubeis, T. Le Marchand, L. B. Andreas, G. Pintacuda, 1H magic-angle spinning NMR evolves as a powerful new tool for membrane proteins. *J. Magn. Reson.* **287**, 140–152 (2018).
26. D. Good, C. Pham, J. Jagas, J. R. Lewandowski, V. Ladizhansky, Solid-state NMR provides evidence for small-amplitude slow domain motions in a multispanning transmembrane α-helical protein. *J. Am. Chem. Soc.* **139**, 9246–9258 (2017).
27. D. Mance, T. Sinnige, M. Kaplan, S. Narasimhan, M. Daniëls, K. Houben, M. Baldus, M. Weingarth, An efficient labelling approach to harness backbone and side-chain protons in ^{1}H-detected solid-state NMR spectroscopy. *Angew. Chem. Int. Ed.* **54**, 15799–15803 (2015).
28. J. Medeiros-Silva, D. Mance, M. Daniëls, S. Jekhmane, K. Houben, M. Baldus, M. Weingarth, ^{1}H-detected solid-state NMR studies of water-inaccessible proteins in vitro and in situ. *Angew. Chem. Int. Ed. Engl.* **55**, 13606–13610 (2016).
29. S. Bernèche, B. Roux, A gate in the selectivity filter of potassium channels. *Structure* **13**, 591–600 (2005).
30. M. Weingarth, E. A. W. van der Cruijsen, J. Ostmeyer, S. Lievestro, B. Roux, M. Baldus, Quantitative analysis of the water occupancy around the selectivity filter of a K^{+} channel in different gating modes. *J. Am. Chem. Soc.* **136**, 2000–2007 (2014).
31. P. W. Fowler, E. Abad, O. Beckstein, M. S. P. Sansom, Energetics of multi-ion conduction pathways in potassium ion channels. *J. Chem. Theory Comput.* **9**, 5176–5189 (2013).
32. S. Jekhmane, J. Medeiros-Silva, J. Li, F. Kümmerer, C. Müller-Hermes, M. Baldus, B. Roux, M. Weingarth, Shifts in the selectivity filter dynamics cause modal gating in K+ channels. *Nat. Commun.* **10**, 123 (2019).
33. J. T. Brennecke, B. L. de Groot, Mechanism of mechanosensitive gating of the TREK-2 potassium channel. *Biophys. J.* **114**, 1336–1343 (2018).
34. W. Lee, M. Tonelli, J. L. Markley, NMRFAM-SPARKY: Enhanced software for biomolecular NMR spectroscopy. *Bioinformatics* **31**, 1325–1327 (2015).
35. W. F. Vranken, W. Boucher, T. J. Stevens, R. H. Fogh, A. Pajon, M. Llinas, E. L. Ulrich, J. L. Markley, J. Ionides, E. D. Laue, The CCPN data model for NMR spectroscopy: Development of a software pipeline. *Proteins* **59**, 687–696 (2005).
36. E. F. Pettersen, T. D. Goddard, C. C. Huang, G. S. Couch, D. M. Greenblatt, E. C. Meng, T. E. Ferrin, UCSF Chimera—A visualization system for exploratory research and analysis. *J. Comput. Chem.* **25**, 1605–1612 (2004).
37. V. Hornak, R. Abel, A. Okur, B. Strockbine, A. Roitberg, C. Simmerling, Comparison of multiple Amber force fields and development of improved protein backbone parameters. *Proteins* **65**, 712–725 (2006).
38. R. B. Best, X. Zhu, J. Shim, P. E. M. Lopes, J. Mittal, M. Feig, A. D. MacKerell, Optimization of the additive CHARMM all-atom protein force field targeting improved sampling of the backbone ϕ, ψ and side-chain χ_1 and χ_2 dihedral angles. *J. Chem. Theory Comput.* **8**, 3257–3273 (2012).
39. J. B. Klauda, R. M. Venable, J. A. Freites, J. W. O'Connor, D. J. Tobias, C. Mondragon-Ramirez, I. Vorobyov, A. D. MacKerell, R. W. Pastor, Update of the CHARMM all-atom additive force field for lipids: Validation on six lipid types. *J. Phys. Chem. B* **114**, 7830–7843 (2010).
40. J. Huang, S. Rauscher, G. Nawrocki, T. Ran, M. Feig, B. L. de Groot, H. Grubmüller, A. D. MacKerell Jr., CHARMM36m: An improved force field for folded and intrinsically disordered proteins. *Nat. Methods* **14**, 71–73 (2017).
41. E. Lindahl, B. Hess, D. van der Spoel, GROMACS 3.0: A package for molecular simulation and trajectory analysis. *J. Mol. Model.* **7**, 306–317 (2001).
42. B. Hess, C. Kutzner, D. van der Spoel, E. Lindahl, GROMACS 4: Algorithms for highly efficient, load-balanced, and scalable molecular simulation. *J. Chem. Theory Comput.* **4**, 435–447 (2008).
43. S. Páll, M. J. Abraham, C. Kutzner, B. Hess, E. Lindahl, Tackling Exascale Software Challenges in Molecular Dynamics Simulations with GROMACS, in *Solving Software Challenges for Exascale* (Springer, 2015), pp. 3–27; http://link.springer.com/10.1007/978-3-319-15976-8_1.
44. M. J. Abraham, T. Murtola, R. Schulz, S. Páll, J. C. Smith, B. Hess, E. Lindahl, GROMACS: High performance molecular simulations through multi-level parallelism from laptops to supercomputers. *SoftwareX* **1–2**, 19–25 (2015).
45. S. Pronk, S. Páll, R. Schulz, P. Larsson, P. Bjelkmar, R. Apostolov, M. R. Shirts, J. C. Smith, P. M. Kasson, D. van der Spoel, B. Hess, E. Lindahl, GROMACS 4.5: A high-throughput and highly parallel open source molecular simulation toolkit. *Bioinformatics* **29**, 845–854 (2013).
46. D. Van Der Spoel, E. Lindahl, B. Hess, G. Groenhof, A. E. Mark, H. J. C. Berendsen, GROMACS: Fast, flexible, and free. *J. Comput. Chem.* **26**, 1701–1718 (2005).
47. H. J. C. Berendsen, D. van der Spoel, R. van Drunen, GROMACS: A message-passing parallel molecular dynamics implementation. *Comput. Phys. Commun.* **91**, 43–56 (1995).
48. O. Beckstein, J. Domanski, A. Somogyi, GromacsWrapper: v.0.3.3 (2015), doi:10.5281/zenodo.17901.
49. W. Humphrey, A. Dalke, K. Schulten, VMD: Visual molecular dynamics. *J. Mol. Graph.* **14**, 33–38 (1996).

Acknowledgments: The plasmid of the NaK2K construct (NaK D66Y and N68D double mutant) was provided by Y. Jiang. **Funding:** This work was supported by the Leibniz-Forschungsinstitut für Molekulare Pharmakologie (FMP), the Max Planck Society, the Deutsche Forschungsgemeinschaft [DFG (FOR 2518 'Dynlon' Project P3 to H.S. and Project P5 to W.K. and B.L.d.G.)], and the European Research Council [ERC Starting Grant (grant agreement no. 337490) to A.L.]. **Author contributions:** K.H., C.S., D.M., and S.L. produced the protein samples. C.Ö., V.C., and K.H. recorded the solid-state NMR spectra. W.K. and B.L.d.G. performed the MD simulations. C.Ö, K.H., W.K., A.L., H.S., and B.L.d.G. analyzed the data. A.L. conceived this study. C.Ö., K.H., and A.L. wrote the manuscript. All authors commented on the manuscript. **Competing interests:** The authors declare that they have no competing interests. **Data and materials availability:** All data needed to evaluate the conclusions in the paper are present in the paper and/or the Supplementary Materials. The NaK2K chemical shifts have been deposited in the Biological Magnetic Resonance Data Bank (BMRB) under accession code 27746. Raw data may be requested from the authors.

Submitted 15 January 2019
Accepted 21 June 2019
Published 31 July 2019
10.1126/sciadv.aaw6756

Citation: C. Öster, K. Hendriks, W. Kopec, V. Chevelkov, C. Shi, D. Michl, S. Lange, H. Sun, B. L. de Groot, A. Lange, The conduction pathway of potassium channels is water free under physiological conditions. *Sci. Adv.* **5**, eaaw6756 (2019).

ScienceAdvances

The conduction pathway of potassium channels is water free under physiological conditions

Carl Öster, Kitty Hendriks, Wojciech Kopec, Veniamin Chevelkov, Chaowei Shi, Dagmar Michl, Sascha Lange, Han Sun, Bert L. de Groot and Adam Lange

Sci Adv **5** (7), eaaw6756.
DOI: 10.1126/sciadv.aaw6756

Science Advances (ISSN 2375-2548) is published by the American Association for the Advancement of Science, 1200 New York Avenue NW, Washington, DC 20005. The title *Science Advances* is a registered trademark of AAAS.